

Editorial Manager(tm) for Proceedings of the Institution of Mechanical Engineers, Part C,
Journal of Mechanical Engineering Science
Manuscript Draft

Manuscript Number:

Title: Modelling of a Low Temperature Differential Stirling Engine

Article Type: Paper

Section/Category: Thermodynamics and Heat Transfer

Keywords: Sterling engine; theoretical analysis; experimental work; low temperature difference

Corresponding Author: Professor Jorge Kubie, BSc (Eng) PhD DSc (Eng)

Corresponding Author's Institution: Napier University Edinburgh

First Author: A Robson

Order of Authors: A Robson; T Grassie; J Kubie

Abstract: A full theoretical model of a low temperature difference Stirling engine is developed in this paper. The model, which starts from the first principles, gives a full differential description of the major components of the engine: the behaviour of the gas in the expansion and the compression spaces; the behaviour of the gas in the regenerator; the dynamic behaviour of the displacer and the power piston/flywheel assembly. A small fully instrumented the engine is used to validate the model. The theoretical model is in good agreement with the experimental data and describes well all features exhibited by the engine.

Assistant Managing Editor
Journal of Mechanical Engineering Science
Professional Engineering Publishing Ltd
1 Birdcage Walk
London
SW1H 9JJ

15 February 2007

Dear Sir

**Paper for Journal of Mechanical Engineering Science
Modelling of a Low Temperature Differential Stirling Engine by A Robson, T Grassie and J Kubie**

I attach an electronic submission of our paper, entitled '*Modelling of a Low Temperature Differential Stirling Engine*', which we believe to be of interest to the readers of the journal.

The paper presents an investigation of an important problem, related to energy and environmental sustainability. The appropriate section of the Journal would be: *Thermodynamics and Heat Transfer*.

As requested, below is a list of possible referees:

1. Professor Ian Bryden
School of Engineering and Electronics
University of Edinburgh
The King's Buildings
Edinburgh, EH9 3JY
2. Professor David Harrison
Head of Creative Technologies
Glasgow Caledonian University
Cowcaddens Road
Glasgow, G4 0BA
3. Professor Miroslav Jicha
Department of Thermodynamics and Environmental Engineering
Faculty of Mechanical Engineering
Brno University of Technology
Technicka 2896/2
616 69 Brno
Czech Republic
4. Dr Ivor McCourt
Technical Director
Hydrastatic Systems Limited
7 Merchiston Park
Edinburgh, EH10 4PW

Yours faithfully

J Kubie (Professor)

Modelling of a Low Temperature Differential Stirling Engine

A Robson, T Grassie and J Kubie¹

School of Engineering and the Built Environment, Napier University, Edinburgh EH10 5DT, UK

Abstract

A full theoretical model of a low temperature difference Stirling engine is developed in this paper. The model, which starts from the first principles, gives a full differential description of the major components of the engine: the behaviour of the gas in the expansion and the compression spaces; the behaviour of the gas in the regenerator; the dynamic behaviour of the displacer and the power piston/flywheel assembly. A small fully instrumented the engine is used to validate the model. The theoretical model is in good agreement with the experimental data and describes well all features exhibited by the engine.

Key words

Sterling engine, theoretical analysis, experimental work, low temperature difference

¹ Corresponding author (j.kubie@napier.ac.uk)

1. Introduction

The original Stirling engine, which was patented in Edinburgh by Reverend Robert Stirling in 1816 [1], has been subject of many monographs [2 and 3]. The development work of the Stirling engine has continued over the years, but many aspects are not reported because of commercial considerations. One of the most interesting aspects has been the development of the Low Temperature Differential Stirling Engine (LTDSE) by Kolin [4]. This engine operated at a temperature difference of about 20 to 100°C, which was an order of magnitude lower than the operating temperature differences achieved up to that time.

A variant of the Stirling engine, the Ringbom engine, was patented by Ringbom in 1907 [5]. In the Ringbom engine there is no direct connection between the flywheel and the displacer, creating a dynamically resonant system, thus allowing the engine to settle at its optimum operating configuration and conditions. It appears that the discontinuous motion of the flywheel and the displacer is more favourable to approximating the ideal Stirling cycle [4]. Senft [6 and 7] developed the Ringbom engine, using many of the ideas introduced by Kolin [4], so that the engine could operate at very low temperature differences. Such an engine, shown schematically in Figure 1, is considered in this paper. In this configuration these engines are not self-starting, but they can operate at very low temperature differences, thus utilising many sources of waste and low grade heat, such as geothermal energy or process heat, which are widely available.

It is the purpose of this paper to develop a full differential analysis of the engine, termed by Martini as a third order analysis [2], and to validate it on an operational engine. A simplified analysis was developed by Senft [8], but that starts with certain assumptions, which may not obtain in practice, such as that the mass of gas in the engine is constant, and, more importantly, that the motion of the piston is sinusoidal. The differential analysis developed below starts from the first principles. The preparatory work has already been reported elsewhere [9].

Experimental work is described first in Section 2; this is followed by the development of the theoretical model in Section 3, which also summarises the numerical results. This is followed by Discussion and Conclusions in Sections 4 and 5 respectively.

2. Experimental Work

2.1. Apparatus

The engine, shown in detail in Figure 2, is based on the design by Senft [10]. The displacer chamber, 116 mm internal diameter and 29 mm high, is made of three polycarbonate rings, which allow the displacer chamber volume to be changed by adding or removing the individual rings. The base of the displacer chamber, which acts as the hot reservoir, 116 mm internal diameter, 46 mm high and manufactured from aluminium, incorporates tapping for the temperature and pressure sensors. Similarly, the head of the displacer chamber, which acts as the cold reservoir, 116 mm internal diameter, 70 mm high and manufactured from aluminium, incorporates tapping for the temperature and pressure sensors, as well a central opening for the displacer rod, and the opening for the power piston; the centreline of the power piston opening is offset 34 mm from the centreline of the displacer chamber. The size of the base and the head allows sufficient heat capacity to ensure a significant period of operation of the engine. Situated on the top of the head of the displacer chamber is a support structure for the flywheel assembly and the crank disk. The flywheel, made of PVC and 170 mm diameter, has its centreline 115 mm above the top of the displacement chamber. The crank arm and the connecting rod are 11 mm and 65 mm long respectively.

The power piston, 34 mm diameter, 20 mm high and manufactured from aluminium, is placed within the opening of the head, and the connecting rod is joined to it with a pin. When the power piston is in its bottom dead position, its bottom surface is 18 mm above the top of the displacer chamber.

The displacer, 115 mm diameter and 10 mm high, is made from low density foam board. The displacer incorporates 4 equally spaced cylindrical openings, 25 mm in diameter, with their centres 30 mm from the centre of the of the displacer, to house the regenerator. The displacer is joined to the displacer rod, which is 14 mm diameter and has an effective contact length 30 mm long. The displacer rod runs through the central opening of the head of the displacer chamber, with its top face open to atmosphere. The regenerator is constructed from steel wool (wire diameter 0.1 mm, average porosity 95%), packed flush into the four circular openings in the regenerator. The total mass of the steel wool in the four openings is 7.5 g.

In order to protect the displacer assembly from damage on impact with the top or the bottom surface of the displacer chamber and to minimise the losses, 5 mm high and 30 mm outside diameter stubs springs were placed centrally on the bottom and the top surface of the displacer. This modification is unique to this work.

The pertinent physical properties of the main engine components are summarised in Table 1.

2.2. Instrumentation

The temperatures of the base and the head of the displacer chamber, the hot and the cold reservoir respectively, are measured with 5 thermocouples, which are situated as indicated in Figure 2. The pressures in the displacer chamber above the displacer (compression space pressure) and the pressure below the displacer (expansion space pressure) are measured relative to the ambient pressure with two pressure transducer (range of 7000 Pa and refresh rate of 200 Hz). The relative pressure across the displacer is also measured with a pressure transducer (range of 100 Pa and refresh rate of 200 Hz). The positions of the pressure tapings are also shown in Figure 2.

The position of the flywheel is determined optically. An array of 36 equidistant slots, 1.44 mm wide and 7.75 mm deep, is machined into the perimeter of the flywheel. A slotted optical switch, consisting of an infrared diode and optical transistor was used. A second optical switch was used to read the position of the flywheel, corresponding to the bottom dead position of the power cylinder. The response time of the optical switches is sufficiently fast for the observed speeds of the engine. The position of the power piston is then determined from the position of the flywheel by simple geometrical considerations.

The position of the displacer is similarly determined by using an optical switch and a system of slots on an extension of the displacer rod, which is connected to the displacer. However, since in this case the bottom dead position of the displacer is not well defined, this was complemented with photographic and pressure analyses.

The signals from the sensors and transducers were sent to a National Instruments data acquisition card for signal conditioning and data logging, and processed on a PC using Microsoft Excel.

2.3. Technique

The engine is placed on a hot plate, thus allowing the base of the displacer chamber, which acts as the hot reservoir, to heat up to the required uniform temperature. When the required temperature is reached the engine is transferred to its insulating jacket, which extends over the base and the displacer chamber. The head of the engine, the cold reservoir, is exposed to the ambient temperature of 20°C, and remains at this temperature. The flywheel is then started by hand at a given starting angle. All experimental data are gathered comprehensively for the first two minutes, and then for five seconds every 30 seconds until the engine stops. The data are analysed in Microsoft Excel.

2.4. Experimental errors

The experimental errors associated with the thermocouples are given by the manufacturers as 2°C . Similarly, the experimental errors associated with the pressure transducers are given as 2% of full scale deflection, giving the errors of the larger range and smaller range pressure transducers as 140 Pa and 2 Pa respectively.

The experimental errors associated with the position of the flywheel are low, and estimated to be limited by the gap between two slots, which is equal to 10° (equal to 0.17 rad). However, the errors associated with the position of the displacer are relatively higher, but less than 1 mm.

2.5. Experimental results

2.5.1. Observations

The influence of the starting angle was investigated first. Various flywheel start angles were used ranging, starting at the bottom dead position (0 rad) to the top dead position (π rad) in $\pi/4$ rad increments. It was observed that the engine was most likely to continue with self sustained motion if the start angle was between about $\pi/4$ rad and $\pi/2$ rad. For starting angles close to 0 rad the flywheel turns but the engine motion soon decays to stop with little rocking. For starting angles close to and above $\pi/2$ rad, the engine stalls and stops at the top dead position. Hence for sustained operation the starting angle of about $\pi/4$ rad was used.

As is well known, the temperature difference between the hot and the cold reservoir determines the behaviour of the engine. For temperature differences below about 60°C the engine did not sustain the motion (at 20°C there was no discernable motion, at 30°C a slight rocking of the flywheel was observed, between 40°C and 60°C the initial amplitude of the rocking increased with the temperature difference, but the rocking gradually increased, and at about 60°C the rocking was sustained). The engine began to run at about 62°C , when the engine settled at a stable speed of about 160 to 180 rpm. With the temperature difference of about 80°C the engine settled at a stable speed of about 200 to 220 rpm.

2.5.2. Quantitative results

A typical set of experimental results, for nominal temperatures of the hot reservoir, T_H and cold reservoir, T_C of 100°C and 20°C respectively, are shown in Table 2 and Figures 3 to 8. Table 2 shows, that, after the initial transient, the temperature difference, $T_H - T_C$, stays virtually constant, decreasing from about 75°C at $t = 13\text{s}$ to about 70°C at $t = 120\text{s}$.

Figure 3 shows the variations of the position of the power piston, x_P , and the relative expansion pressure, $p_E - p_A$, with the elapsed time, t in the vicinity of $t = 13$ s. These variations are typical for all elapsed time in these conditions, in that the relative expansion pressure is about 180° out of phase with the position of the piston; when the piston is at its bottom dead centre, the relative expansion pressure is at its maximum. Figure 4 shows the variations of the relative expansion pressure, $p_E - p_A$, and the differential pressure, $p_E - p_K$, with the elapsed time, t in the vicinity of $t = 13$ s. These variations are typical for all elapsed time in these conditions, in that the variations of the differential pressure are much faster and generally much lower than the variations of either the relative expansion pressure, p_E , or the relative compression pressure, p_K . Figure 5 shows the variations of the position of the piston, x_P , the position of the centre of the displacer above the bottom of the displacer chamber, x_D , and the differential pressure, $p_E - p_K$, with the elapsed time, t in the vicinity of $t = 13$ s. Once again, these variations are typical for all elapsed time in these conditions. Figures 3 to 5 show that in the vicinity of elapsed time $t = 13$ s, the fundamental frequency of these variations is about 2.75 Hz, indicating that the flywheel is rotating at about 165 rpm.

Figures 6 to 8 show the respective conditions of the Sterling engine in the vicinity of elapsed time $t = 120$ s, giving the fundamental frequency of the variations of about 2.8 Hz, indicating that the flywheel is rotating at about 168 rpm.

3. Theoretical analysis

3.1. Initial considerations

Based on a small number of simplifying assumptions, and derivation of simple kinematic relationships, differential description is developed for all important components of the engine:

- the expansion space
- the compression space
- the displacer
- the piston/flywheel assembly
- the regenerator

The various modelling constants, required for the theoretical analysis, are then determined, the approach to obtaining numerical solutions is briefly described, and a typical selection of theoretical results is presented.

The number of simplifying assumptions is kept to a minimum, thus ensuring that the theoretical analysis is as general as possible. It is generally assumed that

- the working fluid is approximated by perfect gas
- gas flow through all the gaps is laminar
- all coefficient of heat transfer are constant
- pressures and temperature are uniform in the expansion and the compression space
- the connecting rod has no mass

Further assumptions, used in describing the behaviour of the regenerator are discussed in Section 3.6. Finally, for simplicity it is assumed that the engine is positioned vertically. This simplifies the calculations without any loss in rigour.

With reference to Figures 9 and 10, the relationships between various kinematic parameters can be derived. First, it can be shown that the relationships between the angles is given by

$$\sin \alpha = \frac{r}{\ell} \sin \theta \quad (1)$$

$$\cos \gamma = \sin(\theta + \alpha) \quad (2)$$

where θ is the angle of the flywheel, and angles α and γ are given in given in Figure 9. The relationship between the position of the power piston, x_P , and the angle of the flywheel, θ , is given by

$$x_p = h_F - \left[\ell^2 - (r \sin \theta)^2 \right]^{0.5} - r \cos \theta \quad (3)$$

where h_F is the vertical distance between the top of the displacer chamber and the centre of the flywheel, ℓ is length of the connecting rod, and r is the length of the crank arm.

3.2. Expansion space

Conservation of energy in the expansion space shows that the change of in gas energy, ΔE_E , is given by

$$\Delta E_E = (Q_H - Q_{ER})\Delta t - \Delta W_D \quad (4)$$

where Q_H is the heat transfer rate to the gas from the hot reservoir, Q_{ER} is the heat flow rate from the expansion space to the regenerator and W_D is the work done by the gas in the expansion space on the displacer.

Making the usual substitutions, equation (4) can be written as

$$\Delta(c_V m_E T_E) = k_{HH}(T_H - T_E)\Delta t - c_P \dot{m}_R T_1^* \Delta t - p_E A_D \Delta x_D \quad (5)$$

where c_V and c_P are the specific heat of the gas at constant volume and constant pressure respectively, m_E and T_E are the mass and temperature of the gas in the expansion space, k_{HH} is the heat transfer parameter between the hot reservoir and the expansion space, A_D is the cross sectional area of the displacer, and \dot{m}_R is the mass flow rate from the expansion space to the compression space (through the regenerator), given as

$$\dot{m}_R = k_{MR}(p_E - p_K) \quad (6)$$

where k_{MR} is the flow parameter. Since the direction of the mass flow rate, \dot{m}_R , is either from the expansion space to the regenerator (for $p_E > p_K$) or from the regenerator to the expansion space (for $p_E < p_K$), the temperature associated with this flow is either the gas temperature in the expansion space, T_E , for $p_E > p_K$, or the temperature of the gas leaving the regenerator to the expansion space, T_{RE} , for $p_E < p_K$; hence the temperature T_1^* in equation (5) is defined as

$$\begin{aligned} \text{for } p_E > p_K \quad T_1^* &= T_E \\ \text{for } p_E \leq p_K \quad T_1^* &= T_{RE} \end{aligned} \quad (7)$$

Noting further that

$$\frac{dm_E}{dt} = -\dot{m}_R \quad (8)$$

equation (5) can be re-written in differential form as

$$\frac{dT_E}{dt} = \frac{1}{c_V m_E} \left[k_{HH} (T_H - T_E) - p_E A_D \frac{dx_D}{dt} + c_V \dot{m}_R (T_E - T_1^*) - R \dot{m}_R T_1^* \right] \quad (9)$$

Finally, the pressure in the expansion space is determined from the gas law as

$$p_E = \frac{m_E R T_E}{V_E} \quad (10)$$

where V_E is the volume of the expansion space is given by

$$V_E = A_D (x_D - 0.5h_D) \quad (11)$$

where h_D is the height of the displacer.

3.3. Compression space

Conservation of energy in the compression space shows that the change of in gas energy, ΔE_K , is given by

$$\Delta E_K = (-Q_C + Q_{KR} + Q_{KA})\Delta t + \Delta W_D - \Delta W_P \quad (12)$$

where Q_C is the heat transfer rate from the gas to the cold reservoir, Q_{KR} is the heat flow rate from the regenerator to the compression space, Q_{KA} is the heat flow rate from the ambient atmosphere to the compression space, W_D is the work done by the displacer on the gas in the compression space, and W_P is the work done by the gas in the compression space on the power piston.

Similarly to above, equation (12) can be written as

$$\Delta(c_V m_K T_K) = -k_{HC} (T_K - T_C)\Delta t + c_P \dot{m}_R T_2^* \Delta t + c_P \dot{m}_A T_3^* \Delta t + p_K (A_D - A_{DR})\Delta x_D - p_K A_P \Delta x_P \quad (13)$$

where m_K and T_K are the mass and temperature of the gas in the compression space, k_{HC} is the heat transfer parameter between the cold reservoir and the compression space, A_{DR} is the cross sectional

area of the displacer rod, A_p is the cross sectional area of the power piston, and \dot{m}_A is the mass flow rate from the ambient atmosphere to the compression space, given as

$$\dot{m}_A = k_{AK}(p_A - p_K) \quad (14)$$

where k_{AK} is the flow parameter. Since the direction of the mass flow rate, \dot{m}_A , is either from the ambient atmosphere to the compression space (for $p_A > p_K$) or from the compression space to the ambient atmosphere (for $p_A < p_K$), the temperature associated with this flow is either the ambient temperature, T_A , for $p_A > p_K$, or the gas temperature in the compression space, T_K , for $p_A < p_K$; hence the temperature T_3^* in equation (13) is defined as

$$\begin{aligned} \text{for } p_A > p_K \quad T_3^* &= T_A \\ \text{for } p_A \leq p_K \quad T_3^* &= T_K \end{aligned} \quad (15)$$

Similarly to equation (7), the gas temperature T_2^* is defined as

$$\begin{aligned} \text{for } p_E > p_K \quad T_2^* &= T_{RK} \\ \text{for } p_E \leq p_K \quad T_2^* &= T_K \end{aligned} \quad (16)$$

where T_{RK} is the temperature of the gas leaving the regenerator to the compression space.

Noting further that

$$\frac{dm_K}{dt} = \dot{m}_R + \dot{m}_A \quad (17)$$

and using equations (1 to 3), equation (13) can be re-written in differential form as

$$\frac{dT_K}{dt} = \frac{1}{c_V m_K} \left[\begin{aligned} &-k_{HC}(T_K - T_C) + p_K(A_D - A_{DR}) \frac{dx_D}{dt} \\ &-p_K A_p \left\{ \frac{r^2 \sin \theta \cos \theta}{\left[\ell^2 - (r \sin \theta)^2 \right]^{0.5}} + r \sin \theta \right\} \frac{d\theta}{dt} \\ &+ c_V \dot{m}_R (T_2^* - T_K) + R \dot{m}_R T_2^* + c_V \dot{m}_A (T_3^* - T_K) + R \dot{m}_A T_3^* \end{aligned} \right] \quad (18)$$

where R is the gas constant.

Finally, the pressure in the expansion space is determined from the gas law as

$$p_K = \frac{m_K RT_K}{V_K} \quad (19)$$

where V_K is the volume of the compression space is given by

$$V_K = (A_D - A_{DR})(h_C - 0.5h_D - x_D) + A_P(x_P - 0.5h_P) \quad (20)$$

where h_C is the height of the compression chamber and h_P is the height of the power piston.

3.4. Displacer

The motion of the displacer is given by a standard equation

$$m_D \frac{d^2 x_D}{dt^2} = -m_D g + (p_E - p_K)A_D + (p_K - p_A)A_{DR} + F_{DA} \quad (21)$$

subject to

$$h_C - 0.5h_D \geq x_D \geq 0.5h_D \quad (22)$$

where m_D is the total mass of the displacer assembly (the displacer, the regenerator and the displacer rod), g is the gravitational acceleration, condition of equation (22) ensures that the displacer is confined within the displacer chamber, and F_{DA} is the restraining force exerted by the two stub springs in the top and bottom surface of the displacer chamber. If the two springs behave linearly over their whole range, the restraining force can be calculated as

$$\begin{aligned} \text{for } 0.5h_D < x_D < h_{SB} + 0.5h_D & \quad F_{DA} = k_{SB}(h_{SB} + 0.5h_D - x_D) \\ \text{for } h_{SB} + 0.5h_D \leq x_D \leq h_C - h_{ST} - 0.5h_D & \quad F_{DA} = 0 \\ \text{for } h_C - h_{ST} - 0.5h_D < x_D < h_C - 0.5h_D & \quad F_{DA} = k_{ST}(h_C - h_{ST} - 0.5h_D - x_D) \end{aligned} \quad (23)$$

where h_{SB} and h_{ST} are the unrestrained lengths of the bottom and the top stub springs respectively, and k_{SB} and k_{ST} are the constants of the bottom and the top stub springs respectively.

3.5. Power piston/flywheel assembly

Referring to Figures 9 and 10, the equations of motion of the power piston and the flywheel can be written respectively as

$$m_P \frac{d^2 x_P}{dt^2} = -m_P g + (p_K - p_A) A_P - F_R \cos \alpha \quad (24)$$

$$I_F \frac{d^2 \theta}{dt^2} = F_R r \cos \gamma - k_{DF} \frac{d\theta}{dt} \quad (25)$$

where m_P is the mass of the power piston, F_R is the axial force in the connecting rod, I_F is the moment of inertia of the flywheel, and the second term on the right hand side of equation (25) combines all the losses acting on the system. It is assumed that these losses are proportional to the angular velocity of the flywheel, with k_{DF} as the constant loss parameter.

Equations (24 and 25) can be combined to eliminate the axial force in the connecting rod, F_R , in terms of the following differential equation for the angle of the flywheel, θ .

$$\begin{aligned} & \left\{ r^3 m_P \cos \gamma \frac{\sin \theta \cos \theta}{[\ell^2 - (r \sin \theta)^2]^{0.5}} + r^2 m_P \cos \gamma \sin \theta + I_F \cos \alpha \right\} \frac{d^2 \theta}{dt^2} = \\ & - r m_P \cos \gamma \left\{ \frac{(r^2 \sin \theta \cos \theta)^2}{[\ell^2 - (r \sin \theta)^2]^{1.5}} + \frac{r^2 [(\cos \theta)^2 - (\sin \theta)^2]}{[\ell^2 - (r \sin \theta)^2]^{0.5}} + r \cos \theta \right\} \left(\frac{d\theta}{dt} \right)^2 \\ & - r m_P g \cos \gamma + r (p_K - p_A) A_P \cos \gamma - k_{DF} \cos \alpha \frac{d\theta}{dt} \end{aligned} \quad (26)$$

3.6. Regenerator

A simple description of the regenerator is developed below. It is assumed that, as shown in Figure 11, the regenerator consists of N gas-matrix cells, consisting of an axisymmetric arrangements of the gas core and the surrounding matrix. It is further assumed that there is no axial conduction of heat, and that the temperature of the gas and the matrix in each cell are uniform (but not identical).

The derivation of the governing equations is demonstrated on the behaviour of the first cell for the gas flow from the expansion space to the compression space ($p_E > p_K$). Conservation of energy in the gas core of the first cell can be written as

$$\Delta(c_V m_{RC} T_{R1}) = c_P \dot{m}_R T_E \Delta t - c_P \dot{m}_R T_{R1} \Delta t - k_{HRM} (T_{R1} - T_{M1}) \Delta t \quad (27)$$

where m_{RC} is the mass of gas in each cell, T_{R1} and T_{M1} are the temperature of the gas and the matrix in the first cell, and k_{HRM} is the heat transfer parameter between the gas core and the surrounding matrix. The first term on the right hand side is the flow of heat into the gas cell, the second term is the flow of heat out of the gas cell and the third term is the conduction of heat from the gas to the surrounding regenerator matrix. Similarly for the surrounding matrix of the first cell

$$\Delta(c_M m_{MC} T_{M1}) = k_{HRM} (T_{R1} - T_{M1}) \Delta t \quad (28)$$

where m_{MC} is the mass of the surrounding regenerator matrix in each cell and c_M is the specific heat of the regenerator matrix.

The regenerator description can then be given as

$$\text{for } p_E \geq p_K$$

cell 1 (next to the expansion space)

$$\frac{dT_{R1}}{dt} = \frac{c_p \dot{m}_R}{c_V m_{RC}} (T_E - T_{R1}) - \frac{k_{HRM}}{c_V m_{RC}} (T_{R1} - T_{M1}) \quad (29)$$

$$\frac{dT_{M1}}{dt} = \frac{k_{HRM}}{c_M m_{MC}} (T_{R1} - T_{M1}) \quad (30)$$

cells $l = 2$ to N

$$\frac{dT_{R,l}}{dt} = \frac{c_p \dot{m}_R}{c_V m_{RC}} (T_{R,l-1} - T_{R,l}) - \frac{k_{HRM}}{c_V m_{RC}} (T_{R,l} - T_{M,l}) \quad (31)$$

$$\frac{dT_{M,l}}{dt} = \frac{k_{HRM}}{c_M m_{MC}} (T_{R,l} - T_{M,l}) \quad (32)$$

$$\text{for } p_E < p_K$$

cell N (next to the compression space)

$$\frac{dT_{R,N}}{dt} = \frac{c_p \dot{m}_R}{c_V m_{RC}} (T_{R,N} - T_K) - \frac{k_{HRM}}{c_V m_{RC}} (T_{R,N} - T_{M,N}) \quad (33)$$

$$\frac{dT_{M,N}}{dt} = \frac{k_{HRM}}{c_M m_{MC}} (T_{R,N} - T_{M,N}) \quad (34)$$

cells $l = N - 1$ to 1

$$\frac{dT_{R,l}}{dt} = \frac{c_p \dot{m}_R}{c_V m_{RC}} (T_{R,l} - T_{R,l+1}) - \frac{k_{HRM}}{c_V m_{RC}} (T_{R,l} - T_{M,l}) \quad (35)$$

$$\frac{dT_{M,l}}{dt} = \frac{k_{HRM}}{c_M m_{MC}} (T_{R,l} - T_{M,l}) \quad (36)$$

where the subscript l refers to the l -th regenerator cell.

3.7. Initial and boundary conditions

It is assumed that the temperatures of the hot and cold reservoirs are constant throughout the process and equal to T_H and T_C respectively. The temperature and pressure of the gas in the engine are initially ambient, T_A and p_A respectively. The temperature of the regenerator matrix is initially also ambient. The displacer initially rests on the bottom stub spring, and the power piston/flywheel assembly is initially stationary, with the flywheel initially at an angle θ_0 . The process starts at time $t = 0$, when an angular velocity ω is imposed on the flywheel.

3.8. Modelling parameters

The characteristics of the various components, such as their dimensions and masses, are given in Table 1. The standard physical constants used in the modelling are given in Table 3. The remaining parameters, which are given in Table 4, were determined by a combination of analytical and experimental considerations.

The flywheel loss parameter, k_{DF} , was determined by measuring the deceleration of the flywheel/piston assembly, when the engine was unheated and the displacer chamber was open to atmosphere. The flow parameter k_{AK} was calculated by measuring the flow rate from the expansion space to the compression space for a given pressure difference. Similarly, the flow parameter k_{MR} was calculated by measuring the gas flow rate from the compression space to the surrounding atmosphere for a given pressure difference.

Additionally the flow of gas between through the annular space between the displacer and displacer chamber was calculated directly, assuming laminar flow, and a flow parameter equivalent to k_{MR} was determined. This directly calculated value was practically equal to the experimentally determined value, indicating that the flow between the expansion and compression space was mainly through the annular space rather than the regenerator. On that basis the equivalent heat transfer parameter between the gas core and the surrounding matrix in the regenerator, k_{HRM} , was estimated as $2/N$ W/K, where, as pointed out above, N is the number of cells in the regenerator.

The mass of the surrounding regenerator matrix in each regenerator cell, m_{MC} , is the ratio of the regenerator mass and the number of regenerator cells. The mass of gas in each regenerator cell, m_{RC} , was calculated from the average regenerator porosity, gas density and the number of regenerator cells.

The heat transfer behaviour in the expansion and compression spaces is difficult to estimate. However, certain scoping calculations can be undertaken. The estimates are made for heat transfer

between the top surface of the hot reservoir (approximated by a heated horizontal plane) and the expansion space, and it is assumed that the heat transfer parameter for heat transfer from the compression space to the cold plate is the same. Assuming, very conservatively, that the heat transfers from the hot plate to the expansion space natural convection, the heat transfer parameter between hot reservoir and expansion space, k_{HH} , is calculated as about 0.1 W/K. However, considering the flow pattern in the expansion space over the hot plate and the intermittent nature of the flow, it is estimated that the heat transfer parameter, k_{HH} , is at least 0.3 W/K. This value is then used in the theoretical calculations for both k_{HH} and k_{HC} .

3.9. Numerical procedure and sequence of calculations

The equations derived above were discretised using standard techniques, and coded. The following sequence of calculations was used:

- the boundary and initial conditions were specified; in particular the initial angle of the flywheel was set at θ_0 , and the initial angular velocity of the flywheel was set at ω
- the number of regenerator cells, N , was specified
- the time interval, Δt , and the total running time t_T were specified
- the initial position of the displacer was determined from its weight and the constant of bottom stub spring
- the calculations then proceeded in the following recurring sequence: the angle of the flywheel θ , the position of the power piston x_P , the position of the displacer x_D , the gas pressure in the expansion space p_E , the gas pressure in the compression space p_K , the mass of gas in the expansion space m_E , the mass of gas in the compression space m_K , the temperature of the regenerator matrix T_M , the temperature of the regenerator gas T_R , the temperature of the gas leaving the regenerator to the expansion space T_{RE} , the temperature of the gas leaving the regenerator to the compression space T_{RK} , the gas temperature in the expansion space T_E and the gas temperature in the compression space T_K

The sequence was generally terminated when the total running time t_T was reached, but it was sometimes terminated earlier if numerical instabilities occurred.

Since the pressure and position changes during the various transients are fast, the time interval, Δt , had to be short to ensure convergence; the time interval $\Delta t = 10^{-7}$ s was used as a compromise for sufficient accuracy and reasonably fast processing times. Similarly, the number of regenerator cells was set at $N = 2$. The accuracy was checked by investigating the influence of decreased time interval and increased number of regenerator cells.

3.10. Numerical results

The base line for the theoretical calculations was obtained for the initial angle of the flywheel set at $\theta_0 = \pi/4$, and for the initial angular velocity of the flywheel was set at $\omega = 20$ rad/s. The influence of the temperature difference $T_H - T_C$ was systematically investigated.

For temperature differences below about 60°C the engine did not sustain the motion (at 40°C and 50°C the flywheel rotates several times before starting to rock, with the rocking being sustained for longer periods as the temperature difference increases). The engine began to run at about 60°C, when the engine settled at a stable speed of about 80 to 100 rpm. With the temperature difference of about 80°C the engine settled at a stable speed of about 130 rpm.

A typical set of theoretical results, for the temperatures of the hot reservoir, T_H and cold reservoir, T_C of 100C and 20C respectively, are shown in Figures 12 to 17.

Figure 12 shows the variations of the position of the piston, x_P , and the relative expansion pressure, $p_E - p_A$, with the elapsed time, t in the vicinity of $t = 13$ s. These variations are typical for all elapsed time in these conditions, in that the relative expansion pressure is about 180° out of phase with the position of the piston: when the piston is at its bottom dead centre, the relative expansion pressure is at its maximum. Figure 13 shows the variations of the relative expansion pressure, $p_E - p_A$, and the differential pressure, $p_E - p_K$ with the elapsed time, t in the vicinity of $t = 13$ s. These variations are typical for all elapsed time in these conditions, in that the variations of the differential pressure are much faster and generally much lower than the variations of either the relative expansion pressure, $p_E - p_A$, or the relative compression pressure, $p_K - p_A$. Figure 14 shows the variation of the position of the piston, x_P , the position of the displacer, x_D , and the differential pressure, $p_E - p_K$ with the elapsed time, t in the vicinity of $t = 13$ s. Once again, these variations are typical for all elapsed time in these conditions. Figures 12 to 14 show that in the vicinity of elapsed time $t = 13$ s, the fundamental frequency of these variations is about 2 Hz, indicating that the flywheel is rotating at about 120 rpm.

Similarly, Figures 15 to 17 show the respective conditions of the Sterling engine in the vicinity of elapsed time $t = 120$ s, giving the fundamental frequency of the variations of about 2.2 Hz, indicating that the flywheel is rotating at about 130 rpm.

4. Discussion

4.1. Comparison of predictions with experimental data

The theoretical predictions and the experimental data are compared with reference to Figures 15 to 17, and Figures 6 to 8, obtained for nominally identical conditions. The two sets of Figures demonstrate that the theoretical model predicts well all aspects of behaviour exhibited by the actual engine.

The variation of the differential expansion pressure, $p_E - p_A$, is about π rad out of phase with the variation of the position of the power piston, x_P , for both experimental data and the theoretical results (Figures 6 and 15). However, it should be noted, that whereas the amplitude of the theoretical predictions of pressure variation is about 6700 Pa, the corresponding amplitude of the experimental data is about 4500 Pa, or about 30% lower. There are two possible reasons for the error. First, it appears that the crank arm in the Stirling engine slipped during operation by about 10% from 11 mm to 10 mm; had it not, the experimental pressure amplitude would have been closer to the predicted amplitude. Second, it is possible that the external flow parameter, k_{AK} , determined experimentally during a semi-static test, increased during to a higher, dynamic value during the actual operation of the Stirling engine, thus allowing significant external venting of the displacer chamber.

Similarly, the variation of the position of the displacer, x_D , is about π rad out of phase with the variation of the position of the power piston, x_P , for both experimental data and the theoretical results (Figures 8 and 17). However, whilst the variation of the position of the power piston is reasonably sinusoidal, both the experimental data and the theoretical predictions demonstrate several interesting features of the variation of the position of the displacer. First, the displacer dwells for a significant fraction of the periodic time in the top dead position, and for even a longer fraction in the bottom dead position. Second, possibly due to the effects of gravity, the drop of the displacer is much faster than its rise. The rapid rise and fall of the displacer is accompanied by large and rapid changes in the differential pressure, $p_E - p_K$, when the displacer approaches the bottom and the top of the displacer chamber. Finally, the displacer appears to bounce on the top and bottom stub springs, as demonstrated by rapid changes in the differential pressure, $p_E - p_K$.

Figures 7 and 16 show that the theoretically predicted variations of the differential pressure, $p_E - p_K$, are much larger than the experimentally determined variations. The probable reason is, once again, that the dynamic value of the internal flow parameter, k_{MR} , is greater than the experimental value obtained during the semi-static tests. However, both Figures indicate that the differential pressure is positive for about one third of the periodic time.

The theoretical model describes many of the aspects demonstrated by the engine, such as the requirement for the minimum temperature difference $T_H - T_C$ of about 60°C to allow continuous

operation of the engine and the importance of the initial angle of the flywheel θ_0 , which has an influence on whether or not the engine would attain continuous operation, and the direction of the sustained rotation of the flywheel. It appears that the operation of the engine depends on the mass of air in the displacer chamber, which then determines the internal pressure distribution, and the initial mass of the air depends on the initial position of the power piston, or the initial position of the flywheel.

Finally, it should be pointed out that the theoretical model underpredicts the angular velocity of the flywheel in its steady-state sustained running. For example, for the temperature difference $T_H - T_C$ of about 75°C , the theoretical model underpredicts the experimental data by about 25%.

4.2. Further considerations and future work

The theoretical model, which was developed from the first principles, is in a reasonable agreement with the experimental data. However, further work is required on the description of the regenerator, further evaluation of the various heat transfer parameters and the removal of some of the assumptions, such as the allocation of the internal flow between the regenerator and the annular gap between the displacer and the displacer chamber, modelling of the connecting rod and the allocation of losses.

The theoretical model will then be used to optimise the engine, and to prepare the theoretical foundations for designing a large and simple low temperature differential Stirling engine, which could be used to utilise large available quantities of low grade heat.

5. Conclusions

A theoretical model of a low temperature differential Stirling engine has been developed. A fully instrumented experimental low temperature Stirling engine has been designed to validate the theoretical model. The model is in a good agreement with the experimental results, and confirms several important features of this kind of engine. First, a certain minimum temperature difference is required to allow a sustained operation of the engine. Second, it is shown that the displacer dwells for significant times at the top and bottom of its travel. Third, the displacer is about 180 degrees out of phase with the power piston. Finally, for a given temperature difference the final angular velocity of the flywheel in sustained operation is independent of the initial conditions, but the direction of the rotation of the flywheel is strongly dependent on the initial conditions. The model will be used to design a large and simple low temperature differential Stirling engine.

References

- 1 **Stirling, R.** UK Patent Number 4081 (1816).
- 2 **Martini, W. R.** *Stirling Engine Design Manual*, University Press of the Pacific (2004).
- 3 **Organ, A. J.** *The Regenerator and the Stirling Engine*, John Wiley and Sons (1997).
- 4 **Kolin, I.** Recent developments of the flat plate Stirling engine, *Proceedings of the 21st Intersociety Energy Conversion Engineering Conference*, Paper 869113, San Diego, California, 25 - 29 August (1986).
- 5 **Ringbom, O.** US Patent Number 856 (1907).
- 6 **Senft, J. R.** *Ringbom Stirling Engines*, Oxford University Press (1993).
- 7 **Senft, J. R.** *Introduction to Low Temperature Differential Stirling Engines*, Moriya Press. (1996).
- 8 **Senft, J. R.** A mathematical model for Ringbom engine operation, *Trans ASME – J. Eng Gas Turbines and Power* **107**, 590-595 (1985).
- 9 **Robson, A. and Grassie, T.** Development of a computer model to simulate a low temperature differential Ringbom Stirling engine, *Proceedings of the 12th International Stirling Engine Conference*, Durham, UK, 7 – 9 September (2005).
- 10 **Senft, J. R.** *Miniature Ringbom Engines*, Moriya Press (2000).

Symbols

A_D	cross sectional area of the displacer
A_{DR}	cross sectional area of the displacer rod
A_P	cross sectional area of the power piston
c_M	specific heat of the regenerator matrix
c_V	specific heat of the gas at constant volume
c_P	specific heat of the gas at constant pressure
E_E	energy of gas in expansion space
E_K	energy of gas in compression space
F_{DA}	spring restraining force
F_R	axial force in the connecting rod
g	gravitational acceleration
h_C	height of the compression chamber
h_D	height of the displacer
h_F	distance between the top of displacer chamber and the centre of flywheel
h_P	height of the power piston
h_{SB}	unrestrained length of the bottom stub spring
h_{ST}	unrestrained length of the top stub springs
I_F	moment of inertia of the flywheel
k_{AK}	flow parameter, given by equation (14)
k_{DF}	flywheel loss parameter
k_{HC}	heat transfer parameter between cold reservoir and compression space
k_{HH}	heat transfer parameter between hot reservoir and expansion space
k_{HRM}	heat transfer parameter between the gas core and the surrounding matrix
k_{MR}	flow parameter, given in equation (6)
k_{SB}	spring constant of the bottom stub spring
k_{ST}	spring constant of the top stub spring
ℓ	length of the connecting rod
m_E	mass of gas in the expansion space
m_D	total mass of the displacer assembly
m_K	mass of gas in the compression space
m_M	total mass of the regenerator matrix
m_{MC}	mass of the surrounding regenerator matrix in each cell
m_{RC}	mass of gas in each cell
m_P	mass of the power piston
\dot{m}_A	mass flow rate from the ambient atmosphere to the compression space
\dot{m}_R	mass flow rate from the expansion space to the compression space
N	number of gas-matrix cells in the regenerator
p_A	ambient pressure

p_E	pressure in the expansion space
p_K	pressure in the compression space
Q_C	heat transfer rate from the gas to the cold reservoir
Q_{ER}	heat flow rate from the expansion space to the regenerator
Q_H	heat transfer rate to the gas from hot reservoir
Q_{KA}	heat flow rate from the ambient atmosphere to the compression space
Q_{KR}	heat flow rate from the regenerator to the compression space
r	length of the crank arm
R	gas constant
t	time
t_T	total running time
T_A	ambient temperature
T_C	temperature of the cold reservoir
T_H	temperature of the hot reservoir
T_E	temperature of the gas in the expansion space
T_K	temperature of the gas in the compression space
T_M	temperature of the regenerator matrix
T_{M1}	temperature of the regenerator matrix in the first cell
T_{RE}	temperature of the gas leaving the regenerator to the expansion space
T_R	temperature of the regenerator gas
T_{R1}	temperature of the regenerator gas in the first cell
T_{RK}	temperature of the gas leaving the regenerator to the compression space
T_1^*	temperature of the gas defined by equation (7)
T_2^*	temperature of the gas defined by equation (16)
T_3^*	temperature of the gas defined by equation (15)
V_E	volume of the expansion space
V_K	volume of the compression space
W_D	work by the displacer
W_P	work on the power piston
x_D	position of centre of displacer above the bottom of displacer chamber
x_P	position of centre of power piston above the bottom dead position
α	angle given in Figure 9
γ	angle given in Figure 9
θ	angle of the flywheel, given in Figure 9
θ_0	initial angle of the flywheel
ω	initial angular velocity is imposed on the flywheel

subscripts

l refers to the l -th regenerator cell

Captions to Figures and Tables

Figures

1. Diagram of a Ringbom engine developed by Senft [6, 7].
2. Diagram of the engine investigated in this work.
3. A plot of the experimentally determined variations of the position of the power piston, x_P , and the relative expansion pressure, $p_E - p_A$, with the elapsed time, t in the vicinity of $t = 13$ s.
4. A plot of the experimentally determined variations of the relative expansion pressure, $p_E - p_A$, and the differential pressure, $p_E - p_K$, with the elapsed time, t in the vicinity of $t = 13$ s.
5. A plot of the experimentally determined variations of the position of the piston, x_P , the position of the centre of the displacer above the bottom of the displacer chamber, x_D , and the differential pressure, $p_E - p_K$ with the elapsed time, t in the vicinity of $t = 13$ s.
6. A plot of the experimentally determined variations of the position of the power piston, x_P , and the relative expansion pressure, $p_E - p_A$, with the elapsed time, t in the vicinity of $t = 120$ s.
7. A plot of the experimentally determined variations of the relative expansion pressure, $p_E - p_A$, and the differential pressure, $p_E - p_K$, with the elapsed time, t in the vicinity of $t = 120$ s.
8. A plot of the experimentally determined variations of the position of the piston, x_P , the position of the centre of the displacer above the bottom of the displacer chamber, x_D , and the differential pressure, $p_E - p_K$ with the elapsed time, t in the vicinity of $t = 120$ s.
9. Nomenclature used in the analysis of the kinematic relationships.
10. Nomenclature used in the analysis of the engine.
11. Approximation of the regenerator used in the analysis.
12. A plot of the theoretically calculated variations of the relative expansion pressure, $p_E - p_A$, and the differential pressure, $p_E - p_K$, with the elapsed time, t in the vicinity of $t = 13$ s.
13. A plot of the theoretically calculated variations of the relative expansion pressure, $p_E - p_A$, and the differential pressure, $p_E - p_K$, with the elapsed time, t in the vicinity of $t = 13$ s.

14. A plot of the theoretically calculated variations of the position of the piston, x_p , the position of the centre of the displacer above the bottom of the displacer chamber, x_D , and the differential pressure, $p_E - p_K$ with the elapsed time, t in the vicinity of $t = 13$ s.
15. A plot of the theoretically calculated variations of the position of the power piston, x_p , and the relative expansion pressure, $p_E - p_A$, with the elapsed time, t in the vicinity of $t = 120$ s.
16. A plot of the theoretically calculated variations of the relative expansion pressure, $p_E - p_A$, and the differential pressure, $p_E - p_K$, with the elapsed time, t in the vicinity of $t = 120$ s.
17. A plot of the theoretically calculated variations of the position of the piston, x_p , the position of the centre of the displacer above the bottom of the displacer chamber, x_D , and the differential pressure, $p_E - p_K$ with the elapsed time, t in the vicinity of $t = 120$ s.

Tables

1. Dimensions and properties of the main engine components.
2. Temperatures of the hot and the cold reservoirs.
3. Physical constants used in the analysis.
4. Additional parameters used in the analysis.

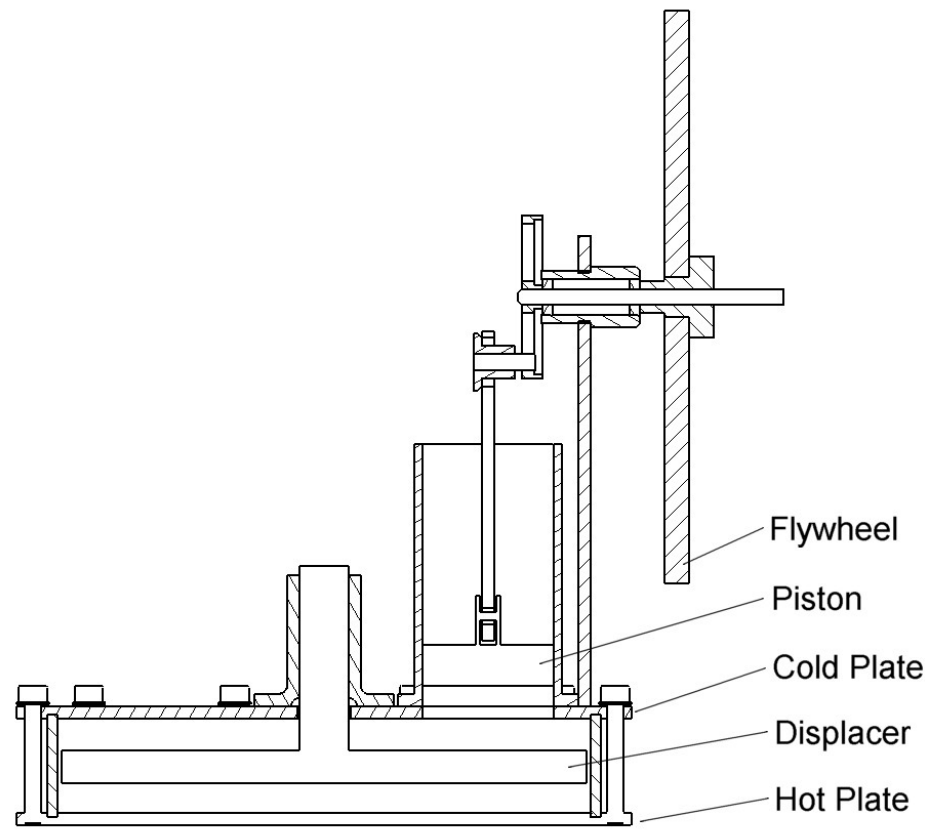


Figure 1

Figure 02

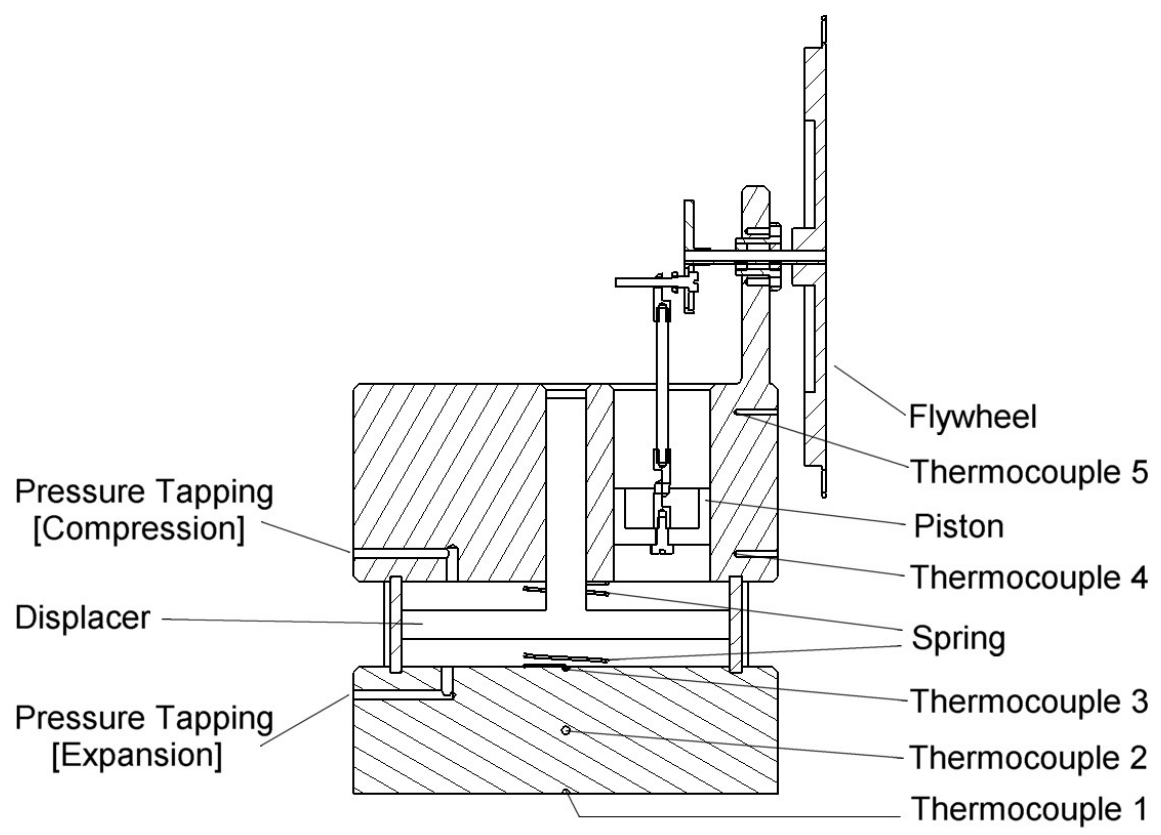


Figure 2

Figure 03

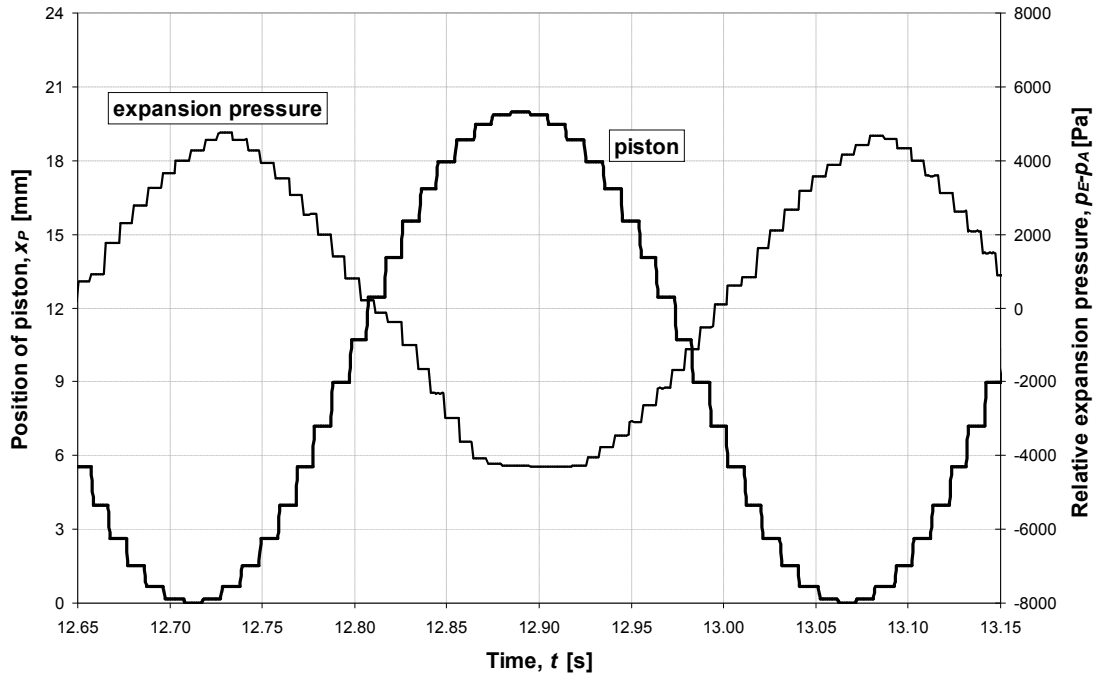


Figure 3

Figure 04

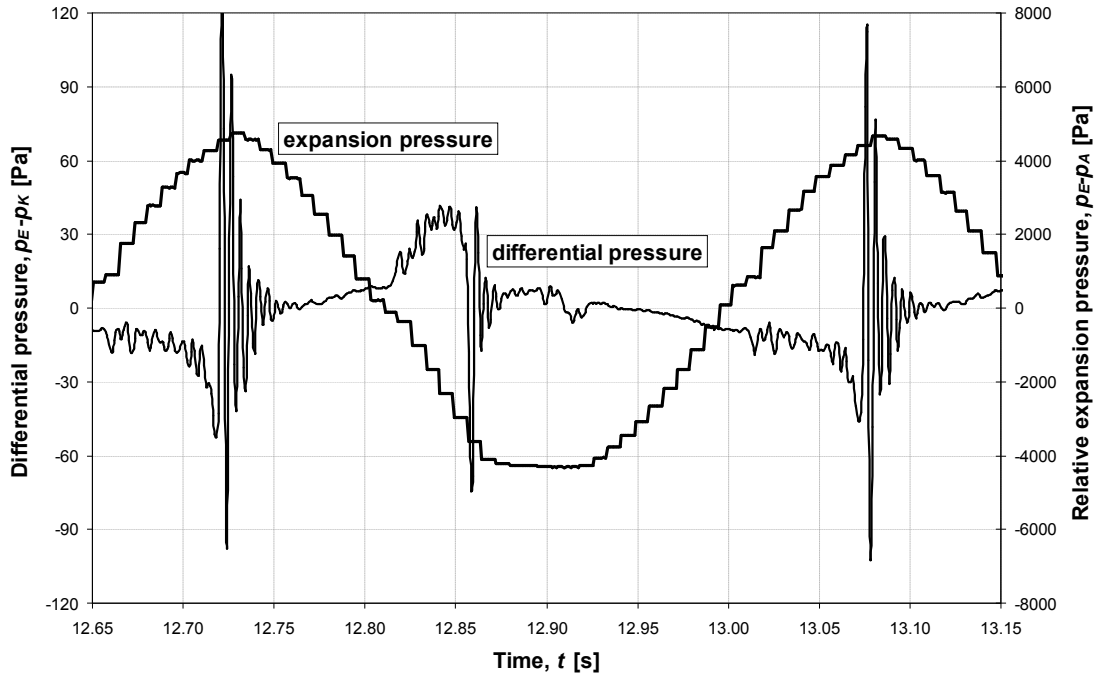


Figure 4

Figure 05

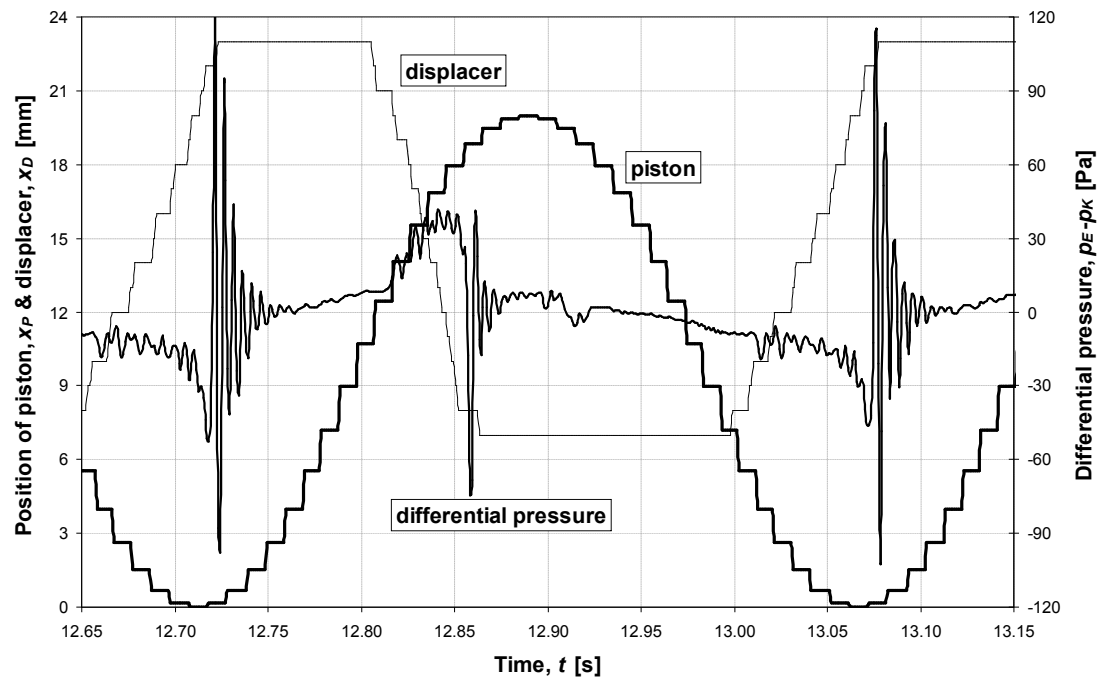


Figure 5

Figure 06

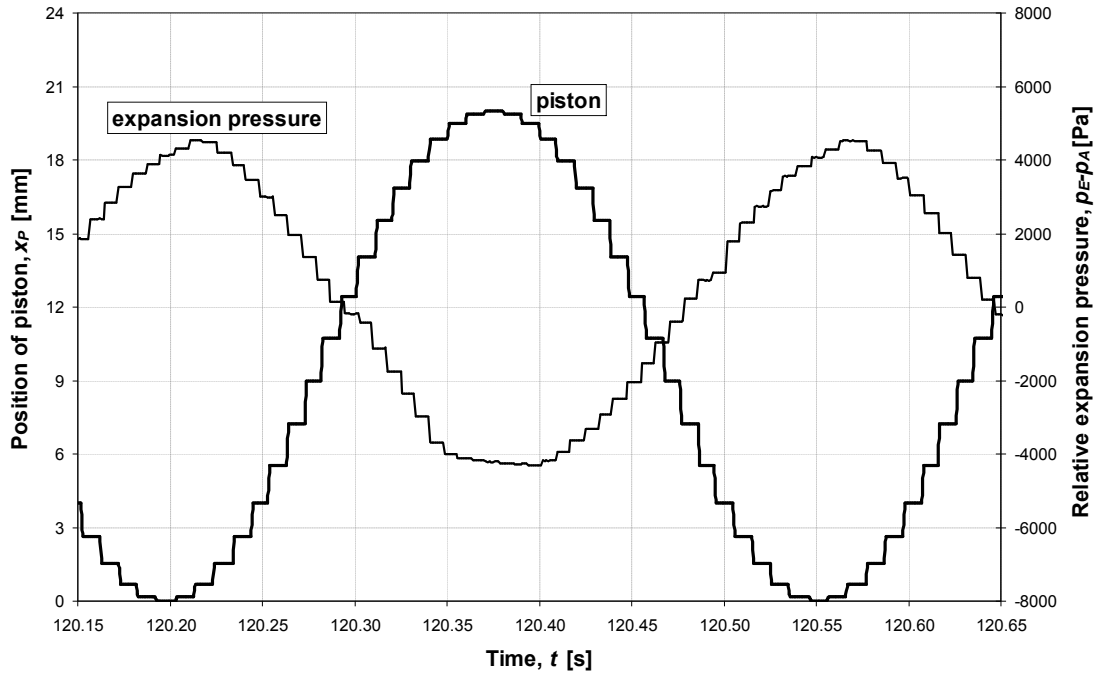


Figure 6

Figure 07

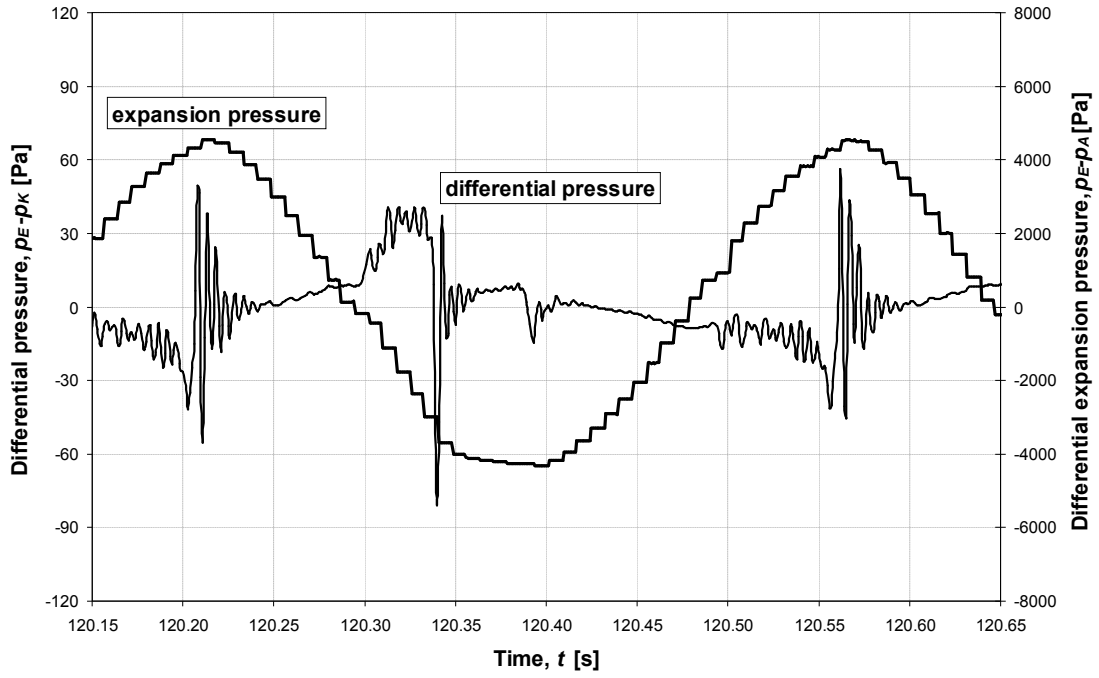


Figure 7

Figure 08

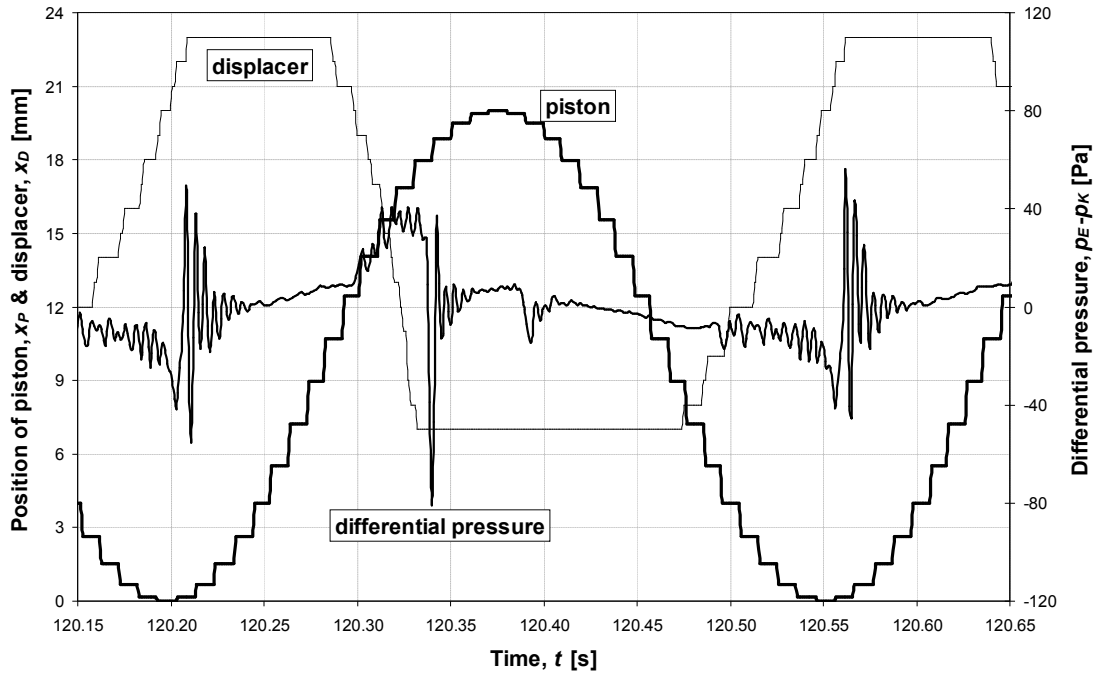


Figure 8

Figure 09

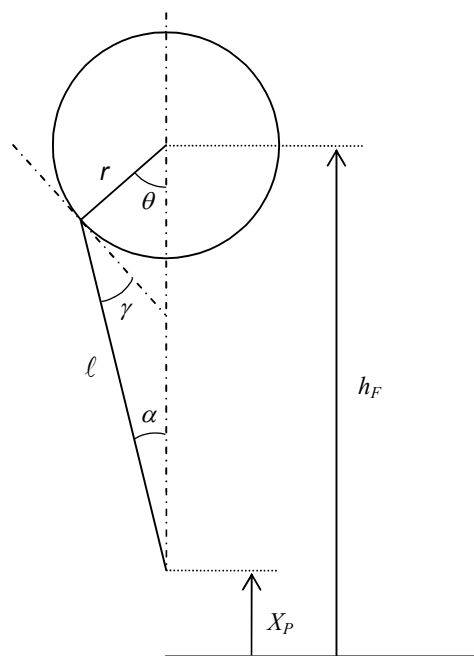


Figure 9

Figure 10

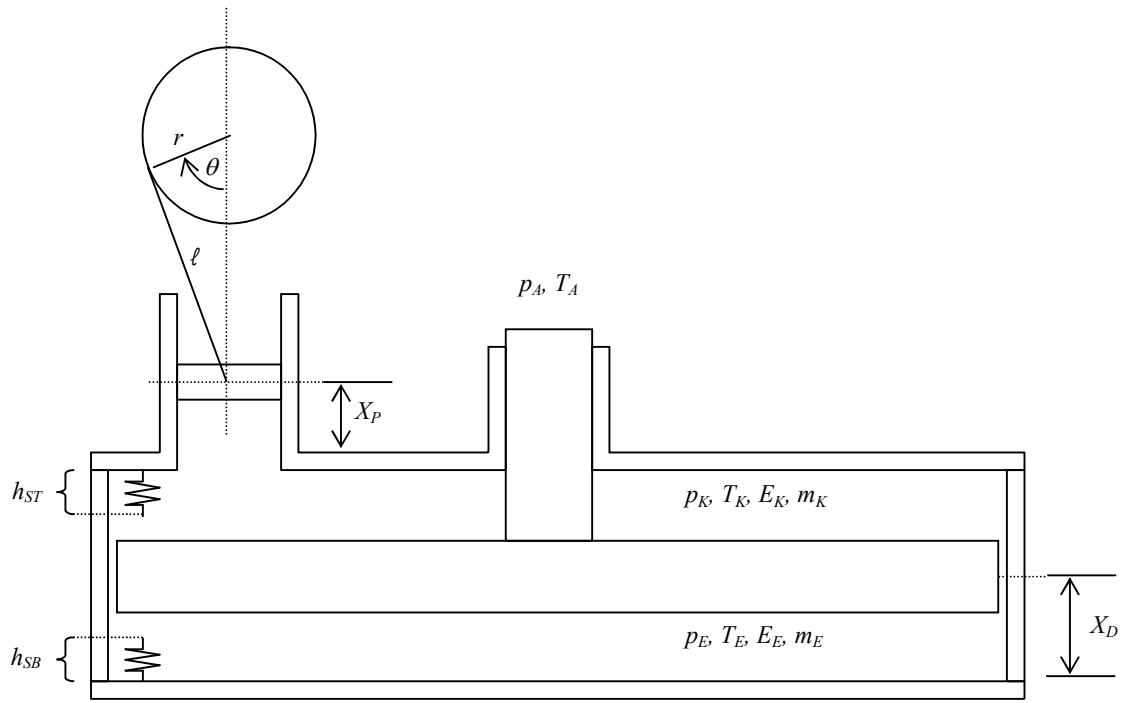


Figure 10

Figure 11

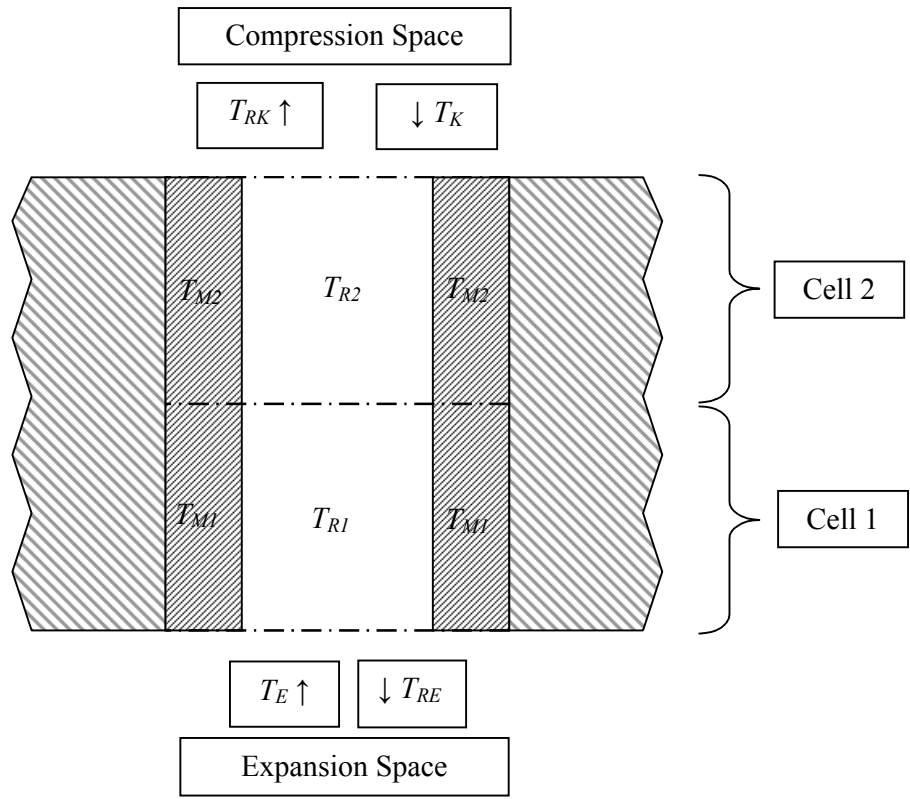


Figure 12

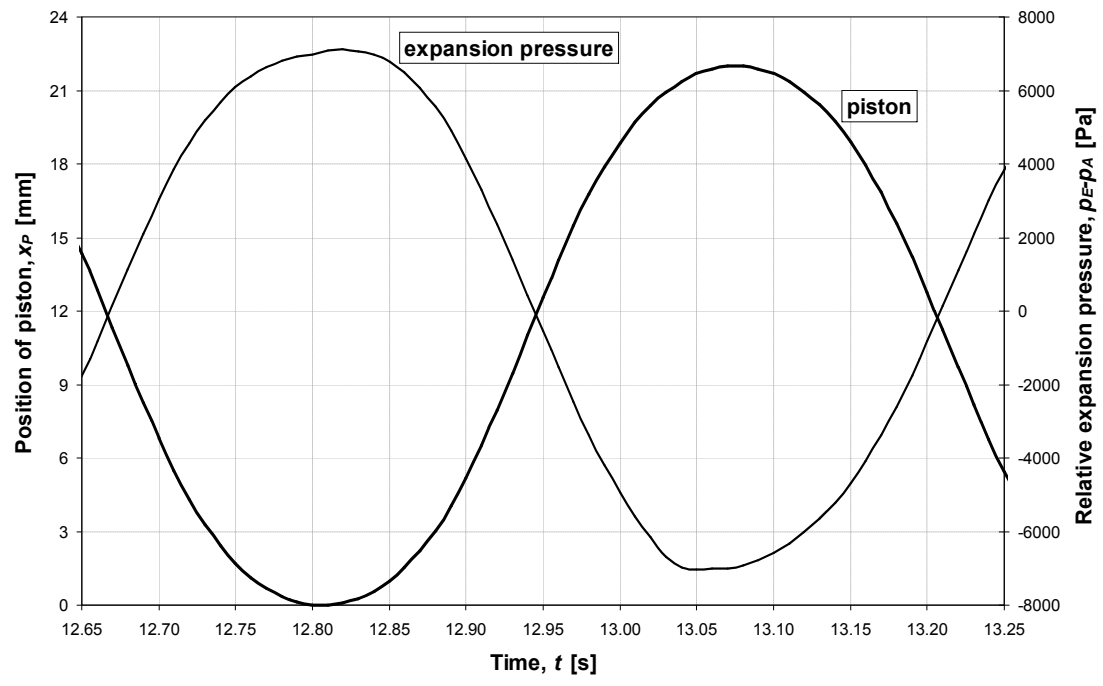


Figure 12

Figure 13

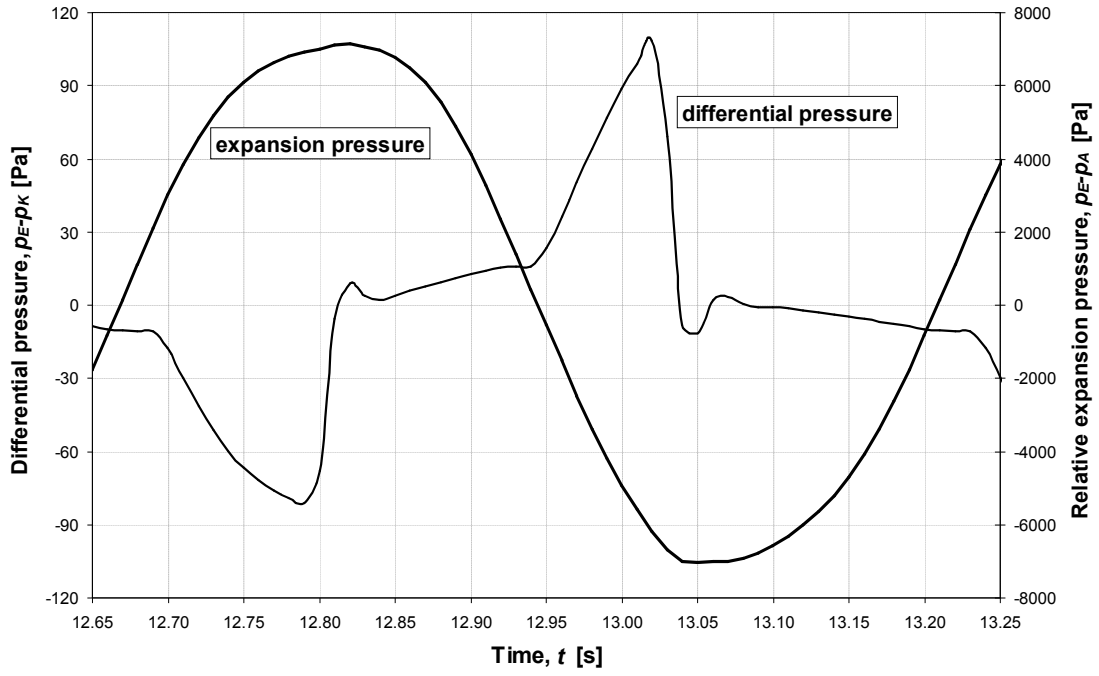


Figure 13

Figure 14

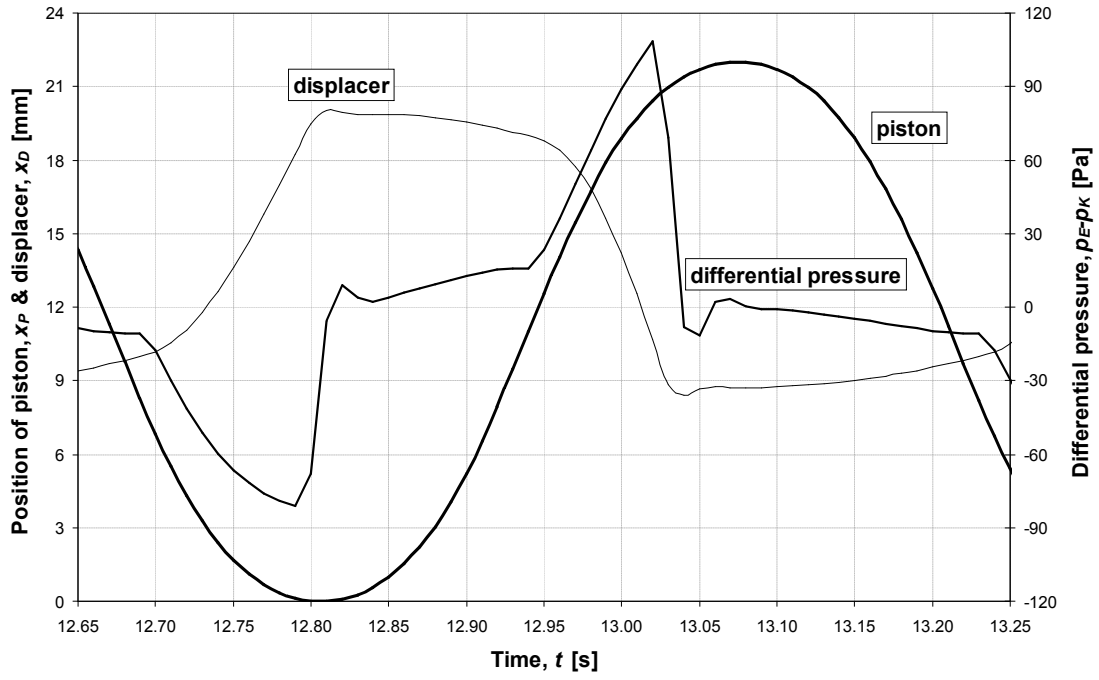


Figure 14

Figure 15

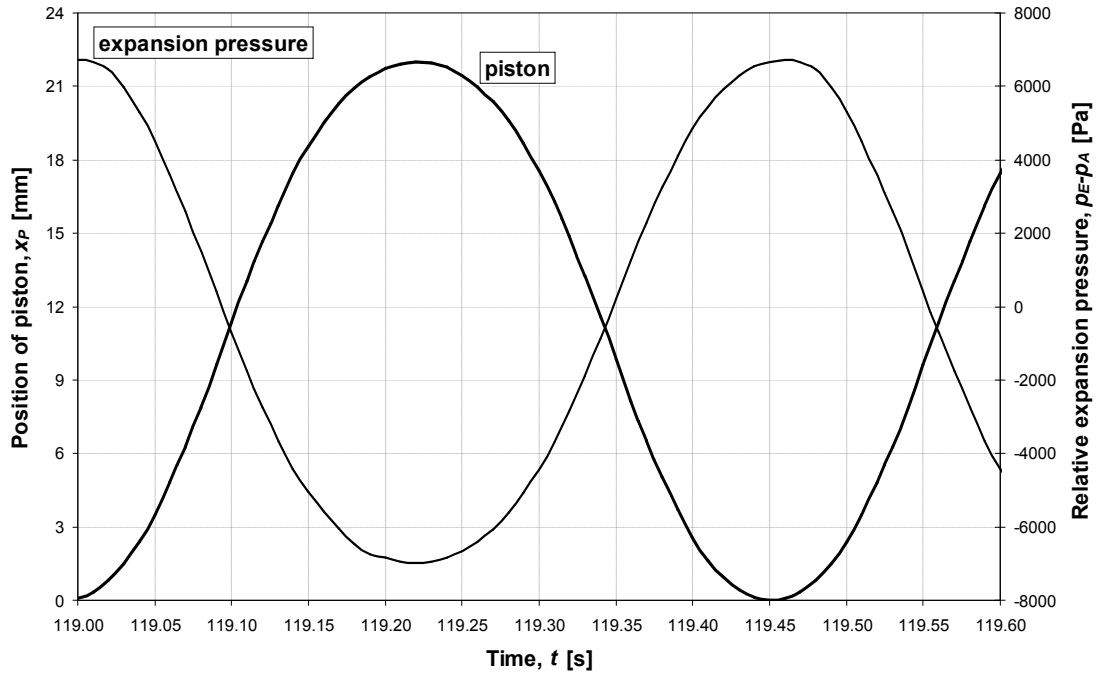


Figure 15

Figure 16

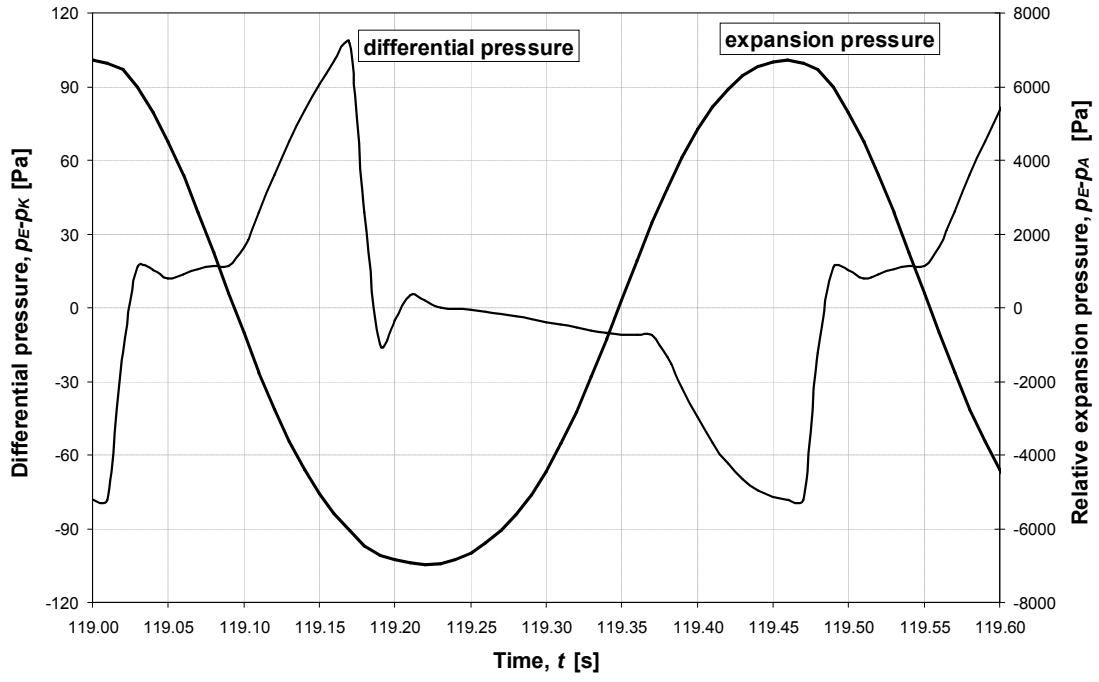


Figure 16

Figure 17

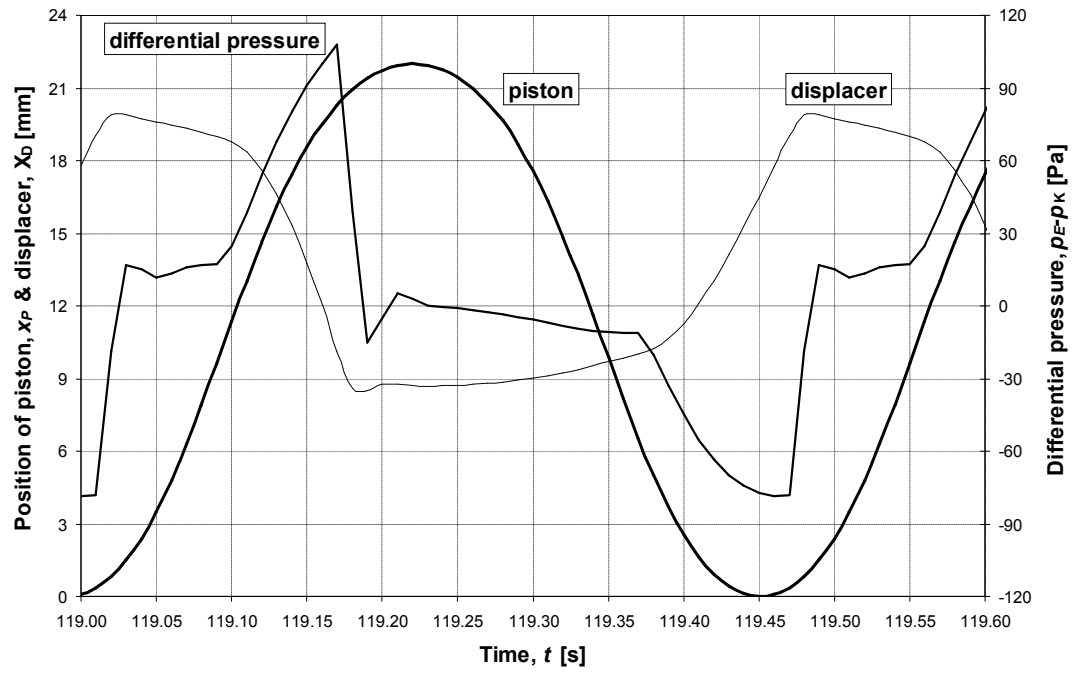


Figure 17

Table 01

Component	Property	Value	Unit
Displacer chamber	Diameter	0.116	m
	Height	0.029	m
Displacer and regenerator assembly	Diameter	0.115	m
	Height	0.010	m
	Mass	0.034	kg
Displacer rod	Diameter	0.014	m
Regenerator segments	Number	4	-
	Diameter	0.020	m
	Height	0.010	m
	Mass (total)	0.0075	kg
	Porosity	95	%
Flywheel	Diameter	0.170	m
	Moment of inertia	0.00069	kg m ²
Power piston	Diameter	0.034	m
	Height	0.020	m
	Mass	0.030	kg
Bottom and top stub springs	Unrestrained length	0.005	m
	Spring constants	1000	N/m

Table 1

Table 02

	Temperature [C]		
	Hot reservoir, T_H	Cold reservoir, T_C	Difference, $T_H - T_C$
nominal	100.0	20.0	80.0
at $t = 0$ s	105.0	16.0	89.0
at $t = 3$ s	96.5	17.0	79.5
at $t = 13$ s	91.0	16.5	74.5
at $t = 22$ s	90.5	16.5	74.0
at $t = 120$ s	87.5	17.0	70.5

Table 2

Table 03

Parameter	Value	Unit
specific heat of the regenerator matrix	450	J/kg K
specific heat of the gas at constant volume	1005	J/kg K
specific heat of the gas at constant pressure	718	J/kg K
gravitational acceleration	9.81	m/s ²
ambient pressure	101000	Pa
gas constant	287	J/kg K
ambient temperature	280	K

Table 3

Parameter	Symbol	Value	Unit
flow parameter, given by equation (14)	k_{AK}	5×10^{-10}	kg/s Pa
flywheel loss parameter	k_{DF}	1×10^{-5}	J s/rad
heat transfer parameter between cold reservoir and compression space	k_{HC}	0.3	W/K
heat transfer parameter between hot reservoir and expansion space	k_{HH}	0.3	W/K
heat transfer parameter between gas core and surrounding matrix	k_{HRM}	$2/N$	W/K
flow parameter, given in equation (6)	k_{MR}	2×10^{-5}	kg/s Pa
mass of the surrounding regenerator matrix in each cell	m_{MC}	$7.5 \times 10^{-3}/N$	kg
mass of gas in each cell	m_{RC}	$2.2 \times 10^{-5}/N$	kg

Table 4